IN-VENTO 2026
International Conference of the Italian Association for Wind Engineering
Bari, September 13th – 16th, 2026
BARI

Modal damping identification of a suspension bridge hanger under different damper configurations

G. Bacci[1], Ø. W. Petersen[1], V. Denoël[2], O. Øiseth[1]

[1]NTNU, Norwegian University of Science and Technology, Trondheim, Norway,
giacomo.bacci@ntnu.no
[2]ULiège, University of Liège, Liège, Belgium

SUMMARY
A full-scale experimental campaign was conducted on the first hanger of the Hålogaland Bridge in Narvik, Norway, to improve the mitigation of vortex-induced vibrations. The objective was to quantify modal damping under different Stockbridge damper configurations. Impact hammer tests were performed at three excitation heights, with responses measured at three locations along the hanger. Closely spaced modes and low structural damping made modal identification challenging. Complementary frequency-domain and time-domain methods provided consistent estimates of bare-hanger damping. The dampers increased modal damping primarily within their dynamically active frequency range, with comparatively little influence outside this band. The effect of both the number and attachment position of the dampers on the distribution of damping across the frequency range is investigated. The results provide full-scale evidence to support the optimisation of damper placement for vortex-induced vibration control.

Keywords: Modal damping, Stockbridge dampers, Vortex-induced vibration

1 INTRODUCTION

Reliable estimates of modal damping in bridge hangers are essential for predicting and mitigating vortex-induced vibrations (VIV). However, full-scale damping data for suspension-bridge hangers remain scarce and estimates often rely on simplified analytical models. For the Hålogaland Bridge, hanger damping was estimated in previous works using a semi-empirical approach (Larsen et al., 2022) based on wind-tunnel data and originally developed for overhead power lines (Rawlins, C., 1998). Earlier work predicted the modal damping of stay cables by solving a complex eigenvalue problem for a taut-string model (Main and Jones, 2001). More recently, a frequency-domain approach was used to identify modal damping ratios from impact hammer tests on the hangers of the Hardanger Bridge (Cantero et al., 2018).

Two challenges complicate such investigations. First, suspension-bridge hangers have closely spaced modes, often with fundamental frequencies below 1 Hz, which makes modal separation and damping identification difficult. Second, aerodynamic damping can affect estimates of structural damping. This is particularly problematic for low-frequency modes, for which long observation windows are needed to capture the decay. In the present study, a full-scale impact hammer campaign was conducted under low-wind conditions on a hanger of the Hålogaland Bridge to estimate the damping of the bare hanger and compare the effectiveness of different Stockbridge damper configurations.

2 DESCRIPTION OF THE MEASUREMENT CAMPAIGN

The impact hammer campaign was conducted on one of the longest hangers of the Hålogaland Bridge: the first hanger from the south on the western side of the bridge. Three triaxial accelerometers were installed at heights of 2 m, 2.8 m and 8 m above the lower end of the

hanger. Impacts were applied at heights of 3.8 m, 5 m and 6.5 m above the same reference point. The measurement and impact locations are shown schematically in Figure 1b.
The impact and measurement locations were selected so that, for each mode up to 60 Hz, at least one excitation point and one measurement point were sufficiently far from a modal node, according to a taut-string approximation of the mode shapes. The hangers have a protective plastic coating to prevent corrosion. Aluminium impact brackets were therefore fitted to protect the coating during hammer testing, as shown in Figure 1a.
The hanger was initially equipped with three Stockbridge dampers (only one is shown in Figure 1a). These were removed to identify the properties of the bare hanger and subsequently reinstalled in the different configurations described in Section 4.

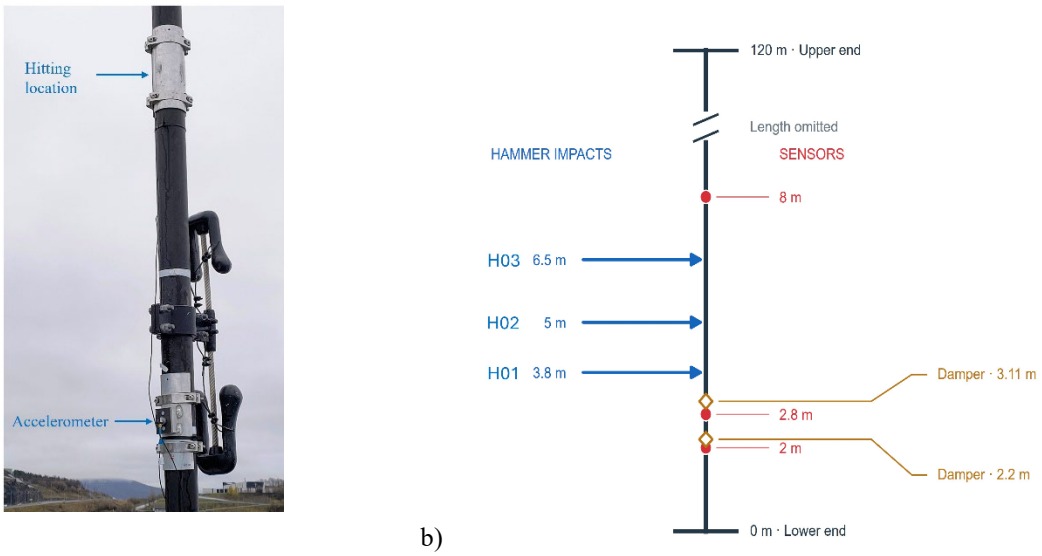

a) b)

Figure 1. (a) Hanger fitted with a Stockbridge damper, an impact bracket and an accelerometer mounted on a measurement bracket. (b) Schematic showing the measurement and impact locations and the damper mounting brackets.

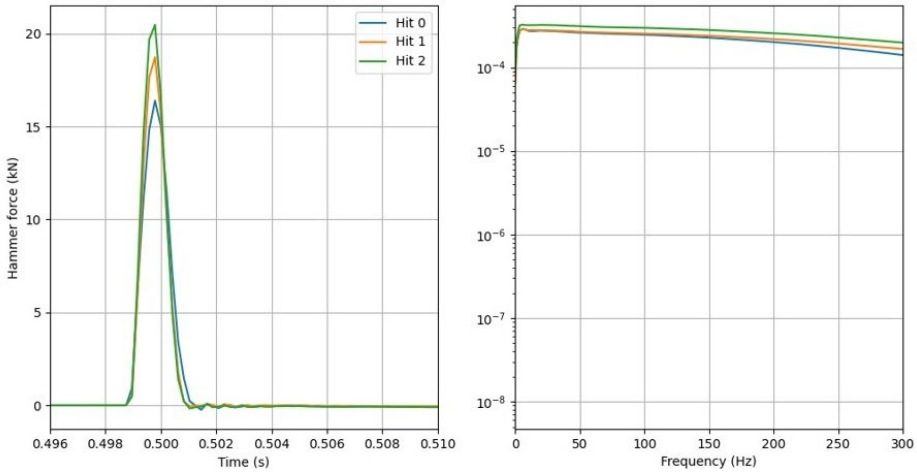

Figure 2. Force time histories and frequency spectra of three hammer impacts at one excitation location.

A 5.5 kg ICP impact hammer fitted with a hard tip was used to excite the hanger. Three impacts were applied at each excitation location. Representative force time histories and frequency spectra for one location are shown in Figure 2. The impacts lasted approximately 2 ms and

reached peak forces of approximately 16 kN. The force spectra were approximately flat over the frequency range of interest, as shown in Figure 2.
The tests were carried out on a morning with a mean wind speed of 1.0 m/s to limit the contribution of aerodynamic damping to the identified damping ratios.

2.1 Estimation of natural frequencies and axial tension

For each analysed response direction, the three excitation positions and three measurement locations provided nine input–output combinations, forming a 3 × 3 frequency response function (FRF) matrix. The FRF for each excitation–response pair was estimated using the H_1 estimator. The hanger's natural frequencies were then identified by peak picking.
For a uniform tensioned beam with simply supported ends, the natural frequency f_n of mode n is related to the mean axial tension T and bending stiffness EI by

$$\frac{f_n}{n} = \frac{1}{2L}\sqrt{\frac{T}{\mu} + \frac{n^2 EI\pi^2}{\mu L^2}}, \tag{1}$$

where μ is the mass per unit length and L is the hanger length. The axial tension and bending stiffness were estimated by fitting this relation to the identified natural frequencies. The fitted model is shown in Figure 3, and the hanger properties and identified parameters are summarised in Table 1.
The identified bending stiffness of approximately 180 kNm² is consistent with tension-dominated behaviour at low mode numbers. The relative contribution of bending stiffness increases with mode number. The low fundamental frequency of approximately 0.8 Hz also implies closely spaced modes, making reliable estimation of structural damping particularly challenging.

Table 1. Hanger properties and parameters identified from impact hammer tests.

Quantity	Symbol	Value	Comment
Hanger length	L	120.2 m	From full-scale hanger data
Aerodynamic diameter	D	0.084 m	From full-scale hanger data
Structural steel diameter	D_{steel}	0.070 m	From full-scale hanger data
Mass per unit length	μ	30 kg/m	From design specifications
Bending stiffness	EI	179.8 kN m^2	From hammer test measurements
Fundamental frequency	f_0	0.787 Hz	From hammer test measurements
Mean axial tension	T_0	1072 kN	From hammer test measurements

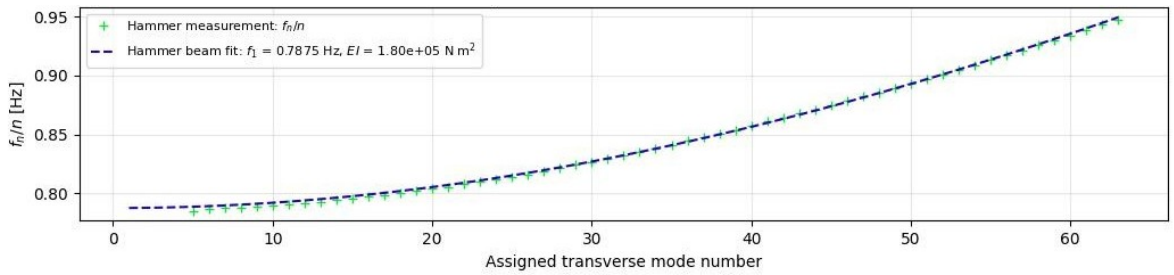

Figure 3. Identified natural frequencies normalised by mode number, f_n/n, and the fitted tensioned-beam model.

3 DAMPING ESTIMATION

Modal damping was identified using two complementary approaches. Circle Fit (CF) is a local frequency-domain method that estimates modal parameters from the complex FRF near each resonance (Cantero et al., 2018). Combined deterministic–stochastic subspace identification (CDS-SI) is a time-domain method that uses the measured hammer force and acceleration responses to identify a state-space model containing several modes simultaneously (Van Overschee and De Moor, 1994). Comparing the two approaches provides a check on estimates obtained from different representations of the same measurements.

3.1 Circle Fit method

The CF method exploits the approximately circular trajectory traced by a complex FRF in the Nyquist plane near a lightly damped resonance. Within a sufficiently narrow frequency interval, the response is assumed to be dominated by a single mode, while the contributions of more distant modes vary slowly with frequency. The procedure is illustrated in Figure 4 for one excitation–response combination.

Figure 4a shows the FRF between excitation location H01 and measurement location A03 (Figure 1b). Peaks were identified using a prominence criterion and a minimum frequency separation of $f_0/2$. A narrow frequency band was then selected around each peak, as illustrated in Figure 4b. A bandwidth of 0.3 Hz was used in this study. The selected FRF segment was plotted in the complex plane, as shown in Figure 4c, and a circle was fitted to its real and imaginary components.

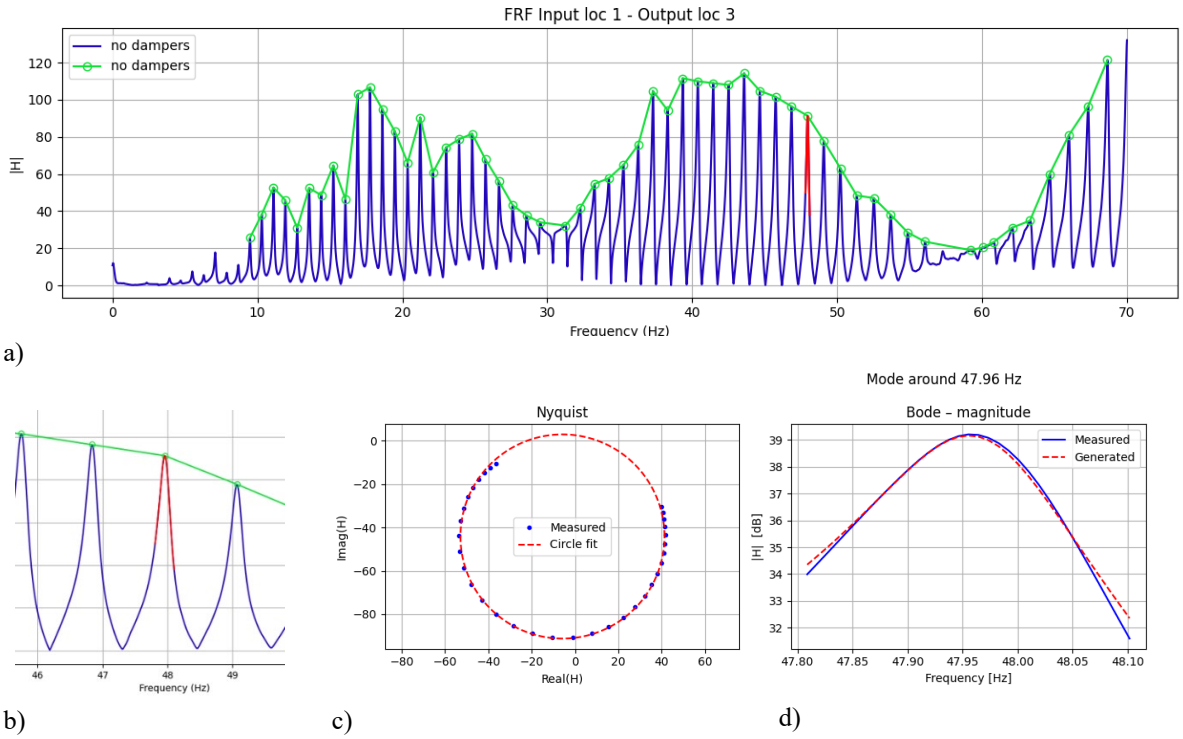

Figure 4. Illustration of the CF procedure for the bare hanger. (a) FRF between excitation location H01 and measurement location A03; identified peaks are marked in green, and the selected peak is highlighted in red. (b) Detail of the selected resonance. (c) Selected FRF points in the complex plane, together with the fitted circle. (d) Comparison of the measured and fitted FRF magnitudes.

Natural frequency and damping are estimated from the distribution of the frequency-labelled FRF points around the fitted circle. Near resonance, the angular position changes rapidly with frequency. For a lightly damped, locally dominant mode, the natural frequency is close to the

frequency at which this angular rate is greatest. Damping is inferred from the frequency separation and corresponding angular separation of points on either side of resonance using Equation (2).

$$\eta_n = \frac{f_a^2 - f_b^2}{f_n^2} \frac{1}{\tan\frac{\theta_a}{2} + \tan\frac{\theta_b}{2}} \cong 2\xi_n, \tag{2}$$

where the indices a and b denote two points on either side of resonance and f_n is the resonance frequency. For light damping, the loss factor η_n is approximately twice the modal damping ratio ξ_n. A lightly damped mode traverses a large part of the circle over a narrow frequency interval, making the frequency information associated with the points essential.

The fitting bandwidth must therefore balance two requirements: it must contain enough points to define the arc but remain narrow enough to limit interference from neighbouring modes. This balance is particularly important for the hanger because its modes are closely spaced. Estimates can also depend on frequency resolution, record length and measurement noise. A nearly circular arc is consequently a useful consistency check but does not by itself guarantee an unbiased damping estimate.

For each identified mode, damping was estimated separately from the FRFs among the nine excitation–response combinations. The estimates were combined using a two-stage weighting procedure. First, estimates from the three response locations were combined for each excitation location, with weights based on the square root of the fitted circle radius. The resulting estimates were then combined across excitation locations using the aggregate weights. At both stages, robust reweighting reduced the influence of discrepant estimates.

3.2 Combined deterministic–stochastic subspace identification

The measured hammer force and acceleration time histories were also analysed using CDS-SI, implemented in the open-source Python package STRID (Frøseth, 2020). In this formulation, a linear, time-invariant state-space model describes both the response to the measured excitation and the effects of unmeasured disturbances and measurement noise. The discrete-time model is written as

$$\begin{aligned} x_{k+1} &= Ax_k + Bu_k + w_k, \\ y_k &= Cx_k + Du_k + v_k. \end{aligned} \tag{3}$$

Here, x_k is the unmeasured state vector, u_k contains the measured hammer force and y_k contains the measured acceleration responses. The matrices A, B, C and D describe the state evolution, input coupling, output mapping and direct feedthrough, respectively. The terms w_k and v_k represent process disturbances and measurement noise. Time-shifted blocks of the measured inputs and outputs are assembled into block Hankel matrices. Singular value decomposition provides a reduced-dimensional representation from which the state-space matrices can be recovered. Several modes are therefore identified jointly, without fitting individual FRF peaks.

The eigenvalues q_r of the identified discrete-time state matrix A are converted into continuous-time poles λ_r using the sampling interval $\Delta t = 0.002$ s. The undamped natural frequency f_r and modal damping ratio ξ_r are then obtained from

$$\lambda_r = \frac{\ln(q_r)}{\Delta t}, \quad f_r = \frac{|\lambda_r|}{2\pi}, \quad \xi_r = -\frac{\mathrm{Re}(\lambda_r)}{|\lambda_r|}. \tag{4}$$

The model order and number of block rows are important identification choices. Before identification, the data were low-pass filtered at 80 Hz. The analysis used 600 block rows and model orders ranging from 40 to 200.
Physical modes can be distinguished from numerical poles by examining the stability of frequency, damping and mode shape as model order varies on a stabilisation diagram. Agreement with CF estimates provides an additional check.

3.3 Results and literature comparison

The damping estimates obtained using the two methods are shown in Figure 5. Reliable estimates were obtained from approximately 5 Hz upwards. Below this frequency, the measured modal responses were insufficient for reliable damping identification, as illustrated by the example FRF in Figure 4a. Both methods yielded a mean structural damping ratio of $\bar{\xi} = 0.042\%$ over the $5 - 45$ Hz range. The lowest values were approximately $\xi_{min} = 0.025\%$ and occurred between 5 Hz and 15 Hz. Damping gradually increased at higher frequencies, reaching a maximum of approximately $\xi_{max} = 0.08\%$ at 45 Hz.

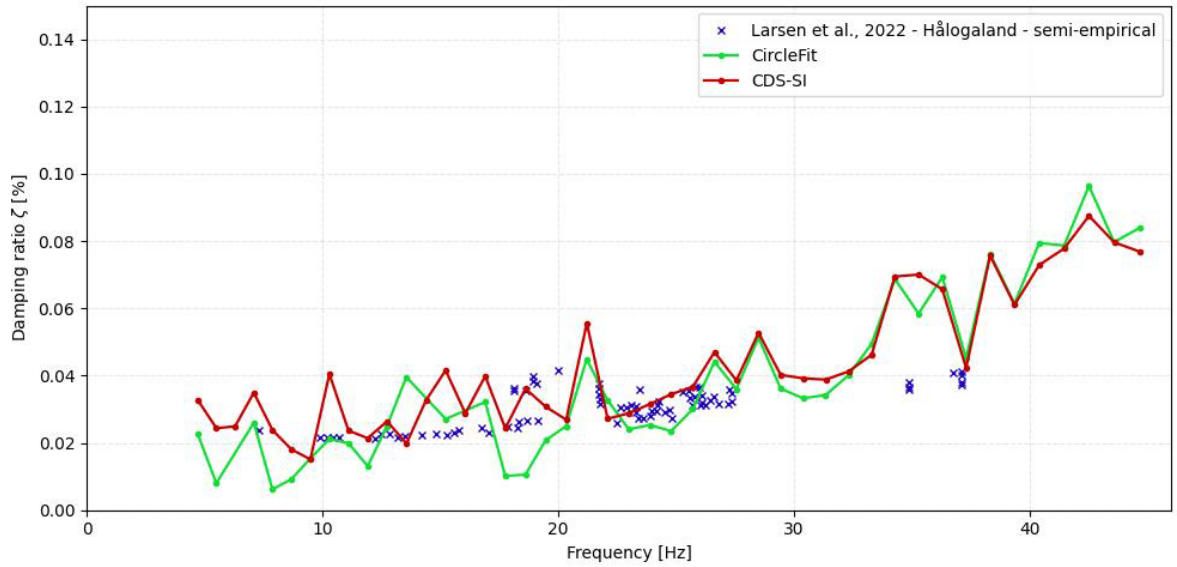

Figure 5. Modal damping ratios identified using CF and CDS-SI, compared with estimates for another hanger of the same bridge (Larsen et al., 2022).

Figure 5 also includes damping estimates from a study of another hanger of the same bridge (Larsen et al., 2022). In that study, structural damping was inferred by inverting a semi-empirical VIV amplitude model, originally developed for overhead power lines, using measured vibration amplitudes. Agreement with the present impact-test estimates supports the reliability of the identified damping values because the two approaches rely on different measurements and modelling assumptions.
The identified damping trend is qualitatively consistent with field observations of VIV on the same hanger (Bacci et al., 2024). That study reported the largest vibration amplitudes when modes in the 5–15 Hz range were excited, corresponding to the range of lowest damping identified here. Vibration amplitudes decreased substantially above 30 Hz, consistent with the higher damping ratios shown in Figure 5.

4 EFFECT OF STOCKBRIDGE DAMPER CONFIGURATIONS

Five damper configurations were investigated using attachment heights of 2 m and 3 m above the lower end of the hanger: three dampers at 3 m; two dampers at 3 m; two dampers, with one at each height; one damper at 2 m; and one damper at 3 m. The attachment locations are shown schematically in Figure 1b, and Figure 6 shows two of the tested configurations. All devices were identical asymmetric Stockbridge dampers. These arrangements allowed the influence of damper number and attachment position on modal damping to be examined. Given the agreement between the identification methods demonstrated in Section 3, CF was selected for this comparison because of its lower computational cost.



a) b)

Figure 6. Two of the tested damper configurations: (a) three dampers at 3 m; (b) two dampers, with one at 2 m and one at 3 m.

The analysis focused on the effective modal damping of the coupled hanger–damper system. The devices exhibit amplitude-dependent behaviour (Bacci et al., 2026), but their nonlinearity was not modelled explicitly in this study. The identified damping ratios therefore represent effective system properties under the excitation conditions of the impact tests.

Figure 7 shows the modal damping ratios identified for the five configurations. The bare-hanger damping estimates from Figure 5 are included as a dashed line in Figure 7 for comparison. The configuration with three dampers at 3 m produced the highest overall damping among the tested arrangements. Its damping curve exhibited three pronounced maxima, consistent with the frequency-dependent resonant response of the asymmetric Stockbridge dampers (Bacci et al., 2026). The dampers show to be effective in the 5-30 Hz frequency range. Reducing the number of dampers from three to two at the same attachment height reduced damping to approximately two-thirds of the three-damper values, while retaining the main features of its frequency dependence. With one damper, damping decreased to approximately one-third of those values. Within the frequency range where the devices were most effective, the mean modal damping ratio decreased from approximately 0.6% for three dampers to approximately 0.2% for one damper.

For the configurations with all dampers at 3 m, differences between configurations were generally small above approximately 30 Hz, and the damping estimates approached those of

the bare hanger. This indicates that, at this attachment height, the dampers made a limited contribution to the damping of the higher modes.
Changing the attachment height altered the distribution of modal damping. Comparisons involving the lower attachment position showed reduced damping in the 5–30 Hz range and a modest increase in the 30–40 Hz range. This behaviour may reflect changes in modal motion at the attachment point. The lower position may lie closer to an antinode of certain higher modes, increasing their coupling with the device, while providing less favourable coupling for modes in the lower frequency range. This interpretation remains tentative and would require comparison with the corresponding mode shapes.

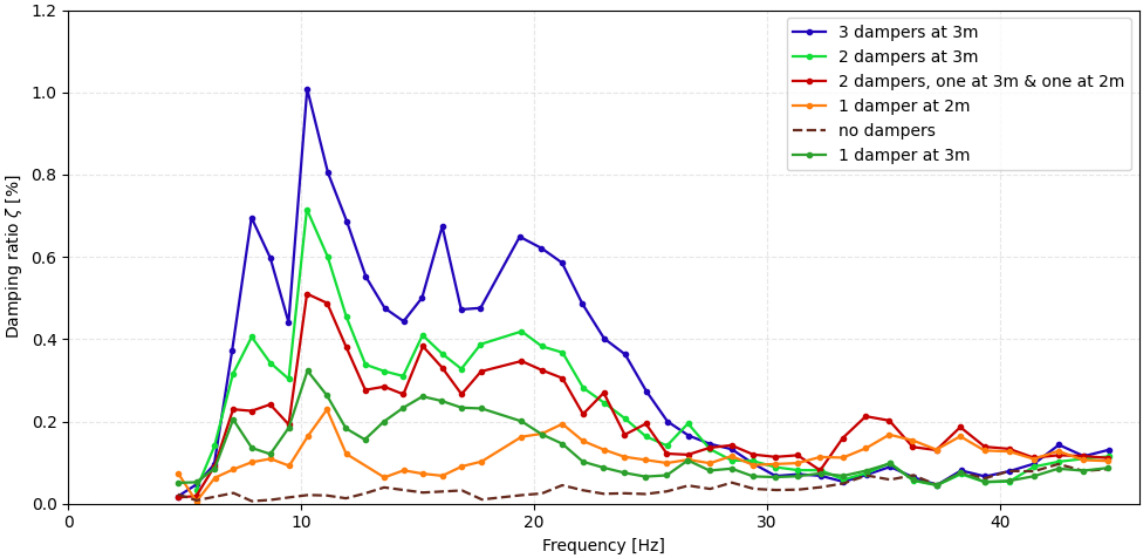

Figure 7. Modal damping ratios of the hanger–damper system identified using CF for five damper configurations. The dashed line shows the bare-hanger damping estimates from Figure 5.

5 CONCLUSIONS

A full-scale impact hammer campaign was conducted on the first hanger of the Hålogaland Bridge in Narvik, Norway, to provide field data for VIV mitigation and damper placement optimisation. The bare hanger's axial tension and bending stiffness were estimated by fitting a tensioned-beam model to the identified natural frequencies. Complementary frequency-domain Circle Fit (CF) and time-domain combined deterministic–stochastic subspace identification (CDS-SI) methods yielded consistent estimates of bare-hanger damping. Agreement with published estimates obtained using a different approach provided additional support for the identified values.
The mean structural damping ratio was $\bar{\xi} = 0.042\%$ over the 5–45 Hz range, with the lowest values, approximately $\xi_{min} = 0.025\%$, occurring below 15 Hz. Damping increased gradually at higher frequencies. These low damping levels help explain the susceptibility of the hanger to VIV in the lower part of the measured frequency range.
The comparison of five Stockbridge damper configurations, performed using CF, showed that both damper number and attachment position affected the distribution of modal damping. Three dampers at 3 m produced the highest overall damping. For devices mounted at this height, damping increased approximately in proportion to damper number within their principal effective frequency range, from 5 Hz to 30 Hz. Lowering the attachment position redistributed the damping contribution between frequency ranges. These results provide full-scale evidence

to inform damper design and placement optimisation for VIV control in suspension-bridge hangers.

ACKNOWLEDGEMENTS
This research was financially supported by the Norwegian Public Roads Administration. The authors gratefully acknowledge this support.

REFERENCES
Bacci, G., Petersen, Ø.W., Denoël, V., Øiseth, O., 2026. Bouc-Wen modelling of asymmetric Stockbridge damper for the wind-induced vibration control of suspension bridge hangers. J. Sound Vib. 626, 119617. https://doi.org/10.1016/j.jsv.2025.119617

Bacci, G., Petersen, Ø.W., Denoël, V., Øiseth, O., 2024. Advanced statistical analysis of vortex-induced vibrations in suspension bridge hangers with and without Stockbridge dampers. J. Wind Eng. Ind. Aerodyn. 255, 105931. https://doi.org/10.1016/j.jweia.2024.105931

Cantero, D., Øiseth, O., Rønnquist, A., 2018. Indirect monitoring of vortex-induced vibration of suspension bridge hangers. Struct. Heal. Monit. 17, 837–849. https://doi.org/10.1177/1475921717721873

Frøseth, G.T., 2020. STRID Python package.

Larsen, A., Andersen, K.G., Jamal, A., 2022. Wind Induced Hanger Vibrations–the Hålogaland Suspension Bridge. Struct. Eng. Int. 32, 62–70. https://doi.org/10.1080/10168664.2021.1930332

Main, J.A., Jones, N.P., 2001. Evaluation of Viscous Dampers for Stay-Cable Vibration Mitigation. J. Bridg. Eng. 6, 385–397. https://doi.org/10.1061/(ASCE)1084-0702(2001)6:6(385)

Rawlins, C., B., 1998. TechnicalNote31-Model of Power Imparted to a Vibrating Conductor by Turbulent Wind.

Van Overschee, P., De Moor, B., 1994. N4SID: Subspace algorithms for the identification of combined deterministic-stochastic systems. Automatica 30, 75–93. https://doi.org/10.1016/0005-1098(94)90230-5